arXiv:0711.4372v1 [astro-ph] 27 Nov 2007

The Elliptical Galaxy NGC 5044: Stellar Population and Ionized Gas

M. G. Rickes[1], M. G. Pastoriza[1] and Ch. Bonatto[1]

Universidade Federal do Rio Grande do Sul (UFRGS), Instituto de Física, Departamento de Astronomia
e-mail: `maurogr@if.ufrgs.br`; `mgp@if.ufrgs.br` and `charles@if.ufrgs.br`

Abstract. In this work we investigate the stellar population, metallicity distribution and ionized gas in the elliptical galaxy NGC 5044, using long-slit spectroscopy and a stellar population synthesis method. We found differences in the slope of metal-line profiles along the galaxy which suggests an enhancement of α elements, particularly towards the central region. The stellar population synthesis showed that the component with $[Z/Z_\odot] \sim 0.0$ dominates the $\lambda 5870$ Å flux in the central region of NGC 5044, contributing with $\sim 42\%$ of the total flux, while in the external regions the contribution decreases to $\sim 8.0\%$. The component with $[Z/Z_\odot] \sim -0.4$ contributes with $\sim 32\%$ in the central region, and $\sim 55\%$ in the external regions. The component with $[Z/Z_\odot] \sim -1.1$ contributes with $\sim 26\%$ in the central region, and $\sim 37\%$ in the external regions. The three components have $\sim 10^{10}$ years. The presence of a non-thermal ionization source, such as a low-luminosity AGN and/or shock ionization, is implied by the large values of the ratio $\frac{[\text{N II}]}{H\alpha}$ observed in all sampled regions. However, the emission lines observed in the external regions indicate the presence of an additional ionization source, probably hot, post-AGB stars.

1. Introduction

A great effort has been made in the last few years to understand how early-type galaxies form and evolve. The relatively recent discoveries that ellipticals are not merely a one-parameter family and that many ellipticals show signatures of interaction with the environment suggest that these galaxies may have different star formation histories, with stellar populations differing in metallicity and/or age (Worthey, Faber & Gonzales 1992).

Crucial information on the above issues has been derived from metal line-strength indices (e.g. Davies et al. 1987) and their radial variation inside the galaxies. The $Mg2$ line-strength distribution in early-type galaxies, for example, can vary considerably, ranging from essentially featureless to structured profiles showing, e.g., changes of slope possibly associated with kinematically decoupled cores, or anomalies in the stellar population of some ellipticals (Carollo et al. 1993).

NGC 5044 is the central and brightest member of a rich group that contains many dE dwarf members and a few Im and Sm dwarf candidates. The mean radial velocity of the group is ~ 2048 km s^{-1} (Ferguson & Sandage 1990). This galaxy presents a very bright ionized gas emission in the form of extended filaments up to 40″ from the center,

being larger in the southern part of the galaxy (Macchetto et al. 1996; Goudfrooij 1991). The dust distribution has an irregular morphology, concentrated in the inner 10″, where two central dark clouds can be seen (Ferrari et al. 1999). NGC 5044 has also been detected by IRAS at 60 and $100\mu m$ and also at 6, 12, and $18\mu m$ by ISO (Ferrari et al. 2002). Its IRAS luminosity is $14 \times 10^8 L_\odot$. The galaxy has a nuclear radio source and extended X-ray emission (Fabbiano et al. 1992) and shows a very complex gas and stellar kinematics. The gas velocity profile is very irregular, with many humps and dips; its radial velocity is systematically blueshifted with respect to the stellar systemic velocity by $\sim 60 - 100$ km s^{-1}. Furthermore, the stellar velocity curves observed on a fairly large area near the galaxy center counter-rotate with respect to the outer regions. Very slow or no stellar rotation is detected along the galaxy's minor axis. The velocity dispersion of the gas peaks at $\sim 200 - 230$ km s^{-1} in the center, decreasing rapidly outwards (Caon et al. 2000). The peculiar kinematics and gas morphology described above may be signatures either of interactions of NGC 5044 with the environment or a post-merger event.

The goal of this paper is to investigate the stellar population, metallicity distribution and the presence of ionized gas in NGC 5044, which are fundamental parameters to understand the formation and evolution of this galaxy.

Parameter	NGC 5044
α(J2000.0)	$13^h15^m23.96^s$
δ(J2000.0)	$-16°23'07.50''$
Morphology	E0
M_B	-21.92
B	11.83
$E(B-V)$	0.070
$L_{H\alpha+[NII]}$ (erg s^{-1})	1.28×10^{41}
Radial velocity (km s^{-1})	2704 ± 33
Redshift	0.00902 ± 0.00011
Diameters (arcmin)	3.0×3.0
H_0 (km s^{-1} Mpc^{-1})	75

Table 1. Data obtained at the NASA/IPAC Extragalactic Database (NED) which is operated by the Jet Propulsion Laboratory, California Institute of Technology, under contract with the National Aeronautics and Space Administration.

This paper is organized as follows: Sect. 2 presents the observations and data reduction; Sect. 3 deals with the equivalent width analysis of the absorption lines and their radial dependence; Sect. 4 describes the stellar population synthesis, whose results are discussed in Sect. 5; Sect. 6 presents an analysis of the emission lines and the nature of the ionization source. Finally, in Sect. 7 a general discussion of the results and conclusions will be drawn.

2. Observations and spectra extraction

NGC 5044 is a bright southern elliptical galaxy for which the general parameters are given in Table 1.

The star formation history, metallicity distribution and emission-gas properties of NGC 5044 are studied using long-slit spectroscopy. The observations were obtained with the ESO 3.6m telescope at La Silla, Chile, equipped with EFOSC1. The spectra cover the range $\lambda\lambda 5100 - 6800$ Å with a 3.6Å/pixel resolution. The spatial scale of the observational configuration is $0.6''$ pixel^{-1}; the slit length was $3.1'$ while its width was fixed at $1.5''$ corresponding approximately to the average seeing; two 2-dimensional spectra were obtained with the same exposition time (approximately 45 minutes) and position angle $PA = 10°$. The slit positioning on the galaxy is shown in Fig. 1 (right panel), in which the dashes mark the spatial location of each extracted spectrum. A final one-dimensional spectrum was obtained combining (by weighted average) the two extractions for each position marked in Fig. 1.

Details on the extracted spectra are given in Table 2. The spectra have been extracted within different areas in order to increase the signal to noise ratio (S/N), since more external regions have lower flux. Each spectrum was corrected for radial velocity ($V_r = 2704$ km s^{-1}) and Galactic extinction ($A_V = 0.07$). The final average spectra, normalized at $\lambda 5870$Å are shown in Fig. 2, separately for the north and south directions on the galaxy.

Table 2. Spatial extractions

Spectra	R (kpc)	R/R_{eff}	Extraction area (kpc)^2
centro	0.00	0	0.06
bN,bS	0.53	11	0.06
cN,cS	1.06	21	0.13
dN,dS	1.59	32	0.19
eN,eS	2.12	43	0.25
fN,fS	2.66	53	0.30
gN,gS	3.19	64	0.30
hN,hS	4.26	85	0.58

Table Notes. Column 2: Distance of the extraction region to the galaxy center. N and S correspond to the north and south directions, respectively.
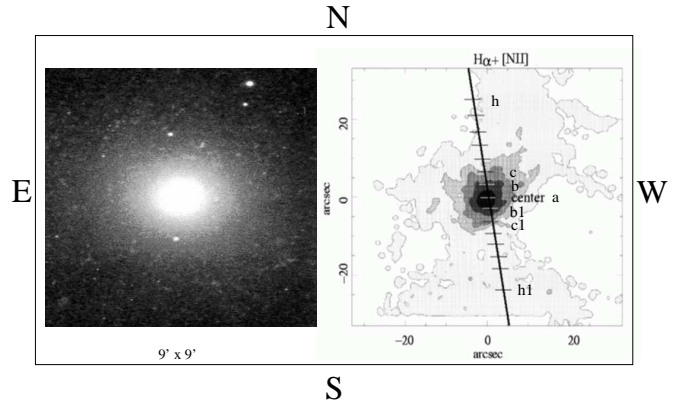

Fig. 1. NGC 5044. Left panel - V band image. Right panel - slit positioning and spatial extraction on an Hα image. Darker gray corresponds to larger flux.

3. Equivalent width and radial dependence

Elliptical galaxies present systematic variations on the line strength indices Mg 2 and Fe I, either from the center to the external regions of a given galaxy or limited to the central regions of different galaxies (cf. Gonzáles 1993; Carollo & Danziger 1994a,b; Carollo et al. 1993; Davies et al. 1993; Fisher et al. 1995, 1996). Furthermore, the gradients in Mg 2 and Fe I have different slopes, suggesting an enhancement of Mg (α elements in general, which are associated with the Super-Novae type I rate) with respect to Fe toward the center of these galaxies. The inferred degree of enhancement seems to increase from dwarfs to massive ellipticals (see Faber et al. 1992, Worthey et al. 1994 and Matteucci 1997).

The above arguments suggest the occurrence of changes in some fundamental properties of the constituent stellar population. In order to investigate if NGC 5044, which presents a peculiar stellar kinematics and external ionized gas filaments, has stellar population and metallicity properties similar to those of other elliptical galaxies, we first investigate the spatial distribution of metal-line strengths, and then perform a stellar population analysis.

The present spectra of NGC 5044 cover the spectral range $\lambda\lambda 5100 - 6800$Å which constrains the number of im-
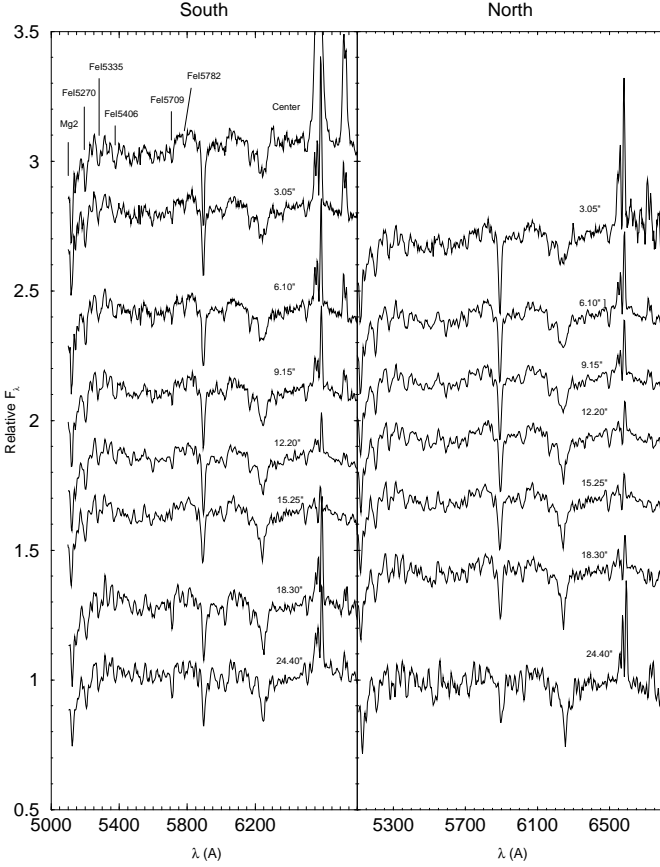
Fig. 2. Spatial extractions for the South (left panel) and North (right panel) directions normalized at $\lambda 5870$ Å. The distance to the galaxy center is indicated on each spectrum. Except for the bottom ones, the spectra have been shifted by an arbitrary constant, for clarity purposes

portant absorption lines used in stellar population studies. However, in this spectral region the galaxy presents several neutral iron lines, e.g. Fe I$_{\lambda 5270}$, Fe I$_{\lambda 5335}$, Fe I$_{\lambda 5406}$, Fe I$_{\lambda 5709}$ and Fe I$_{\lambda 5782}$, as well as the Mg 2 band. These absorption features present strong dependence on the age and metallicity of the underlying stellar population (Bica & Alloin 1986).

Previous to the measurements, all spectra have been normalized at $\lambda 5870$Å. The continuum tracing and spectral windows of the absorption lines used in the present paper are those defined by the Lick system (Faber et al. 1985), which are reproduced in Table 3. Each equivalent width (EW) and the Mg 2 index have been measured three times taking into account the uncertainties in the continuum level definition. This procedure allowed us to estimate the average value and corresponding standard deviation for each measurement.

Although Na I$_{\lambda 5895}$ is the strongest absorption feature present in our spectra, it was not used in the analysis because it may be contaminated by dust concentrated in the central region of the galaxy (Ferrari et al. 1999). Besides the EWs and Mg 2 index, we measured as well continuum points at 5300Å, 5313Å, 5406Å, 5800Å, 5870Å and

Table 3. Lick indices definitions

Index	Line/Band	$\Delta \lambda$ (Å)	AC (Å)
$Mg2_{Band}$	$Mg2$	5155.375—5197.875	4896.375—4958.875
			5302.375—5367.375
$Fe_{\lambda 5270}$	Fe I	5247.375—5287.375	5234.875—5249.875
			5287.375—5319.875
$Fe_{\lambda 5335}$	Fe I	5314.125—5354.125	5306.625—5317.875
			5355.375—5365.375
$Fe_{\lambda 5406}$	Fe I	5390.250—5417.750	5379.000—5390.250
			5417.750—5427.750
$Fe_{\lambda 5709}$	Fe I	5698.375—5722.125	5674.625—5698.375
			5724.625—5738.375
$Fe_{\lambda 5782}$	Fe I	5778.375—5798.375	5767.125—5777.125
			5799.625—5813.375

Table Notes. Column 3: Spectral window; Column 4: Adjacent Continuum.

6630Å, as defined in Bica & Alloin (1986). These continuum points, normalized at $\lambda 5870$ Å, are listed in Table 5.

In order to compare our results for NGC 5044 with other elliptical galaxies which present similar radial gradients in the Mg 2 band and in Fe I$_{5270}$ and Fe I$_{5335}$ lines (e.g. Davies et al., 1987; Carollo et al. 1993), we first corrected these features for the line broadening due to the internal stellar velocity dispersion.

The spectrum of the G giant star HR 5333 was used to estimate the velocity dispersion correction. HR 5333 was assumed to have zero intrinsic velocity and its spectrum was broadened with a series of gaussian filters with a velocity dispersion σ varying from $0 - 300$ km s^{-1}, in steps of 10 km s^{-1}.

For each absorption feature considered we calculate an empirical correction index C(σ), so that $C(\sigma)_{Mg2} = \frac{Mg2(0)}{Mg2(\sigma)}$, and $C(\sigma)_{FeI} = \frac{W_\lambda(0)}{W_\lambda(\sigma)}$. The velocity dispersion in NGC 5044 varies from ~ 260 in the center to ~ 230 $km\, s^{-1}$ in the external regions (Caon et al. 2000). We have calculated the correction index $C(\sigma)$ for each marked position in Fig. 1 using Caon et al.'s (2000) σ values. Our correction factors vary from 1.23 to 1.27 for the Mg 2 index and from 1.20 to 1.23 for the Fe I lines, in the velocity range 230–260 km s^{-1}. Our correction factors for the Mg 2 index are somewhat larger than those given by Davies et al. (1993), while those for Fe I$_{\lambda 5270}$ are similar.

As can be seen in Fig. 3, except for Fe I$_{\lambda 5406}$ (panel(d)), the other absorption features present strong variations with distance to the center. In particular, the Mg 2 band (panel (a)) clearly presents a positive gradient, i.e. increasing towards the center of the galaxy, whereas the other Fe I lines present evidence of negative gradients.

3.1. Metallicity gradient

The radial distributions of the Mg 2 index and those of the EWs of Fe I$_{5270}$, Fe I$_{5335}$, Fe I$_{5406}$, Fe I$_{5709}$ and Fe I$_{5782}$, corrected for velocity dispersion, are shown in Fig. **??**. The corrected Mg 2 index (panel(a)) presents an enhancement of the gradient which decreases from 0.42 mag in the center to ~ 0.32 mag in the external regions of the galaxy. On the other hand, the corrected EW of Fe I$_{5270}$ (panel(b))

Table 4. Mg 2 index and EWs of the Mg 2 and Fe I lines.

R ('')	mag		EW (Å)				
	$\mathrm{Mg\,2}_{index}$	$\mathrm{Mg\,2}_{band}$	$\mathrm{Fe\,I}_{\lambda5270}$	$\mathrm{Fe\,I}_{\lambda5335}$	$\mathrm{Fe\,I}_{\lambda5406}$	$\mathrm{Fe\,I}_{\lambda5709}$	$\mathrm{Fe\,I}_{\lambda5782}$
0	0.416 ± 0.013	13.92 ± 0.51	2.31 ± 0.16	1.14 ± 0.23	0.56 ± 0.01	1.11 ± 0.12	0.89 ± 0.02
3.05S	0.370 ± 0.008	13.33 ± 0.38	2.67 ± 0.11	1.17 ± 0.25	0.96 ± 0.32	1.35 ± 0.03	0.97 ± 0.06
6.10S	0.378 ± 0.001	11.85 ± 0.62	3.11 ± 0.26	1.60 ± 0.50	0.92 ± 0.16	1.46 ± 0.04	1.15 ± 0.20
9.15S	0.339 ± 0.014	11.72 ± 0.70	2.29 ± 0.64	1.21 ± 0.30	0.77 ± 0.24	1.35 ± 0.01	0.93 ± 0.07
12.20S	0.325 ± 0.010	11.20 ± 0.42	3.37 ± 0.01	1.51 ± 0.58	0.96 ± 0.07	1.67 ± 0.24	0.93 ± 0.18
15.25S	0.317 ± 0.014	11.69 ± 0.70	2.87 ± 0.13	1.31 ± 0.30	0.45 ± 0.24	1.45 ± 0.15	0.74 ± 0.23
18.30S	0.364 ± 0.006	11.65 ± 0.51	3.52 ± 0.27	2.57 ± 0.69	0.74 ± 0.22	2.68 ± 0.38	1.41 ± 0.46
24.40S	0.320 ± 0.006	11.23 ± 0.36	3.58 ± 0.62	3.12 ± 0.50	1.22 ± 0.01	2.24 ± 0.26	1.15 ± 0.49
3.05N	0.365 ± 0.017	13.29 ± 0.38	1.99 ± 0.11	2.00 ± 0.25	0.82 ± 0.16	1.08 ± 0.13	0.93 ± 0.13
6.10N	0.364 ± 0.006	12.62 ± 0.62	2.13 ± 0.26	1.67 ± 0.50	0.81 ± 0.07	1.16 ± 0.12	0.85 ± 0.12
9.15N	0.335 ± 0.002	11.47 ± 0.70	1.92 ± 0.12	1.55 ± 0.30	0.63 ± 0.02	0.89 ± 0.12	0.99 ± 0.12
12.20N	0.330 ± 0.007	11.71 ± 0.22	1.93 ± 0.20	1.25 ± 0.58	0.76 ± 0.17	0.78 ± 0.15	0.75 ± 0.15
15.25N	0.330 ± 0.005	11.54 ± 0.17	2.21 ± 0.13	1.16 ± 0.30	0.66 ± 0.20	0.98 ± 0.15	0.64 ± 0.15
18.30N	0.324 ± 0.002	12.33 ± 0.51	2.69 ± 0.27	1.63 ± 0.69	1.37 ± 0.01	1.25 ± 0.01	1.41 ± 0.01
24.40N	0.320 ± 0.010	11.29 ± 0.36	2.92 ± 0.62	1.59 ± 0.50	1.15 ± 0.17	2.05 ± 0.27	0.52 ± 0.27

Table Notes. Column 1: Distance of the extraction to the galactic center. N and S correspond to the north and south directions, respectively.

Table 5. Continuum points

R ('')	C_λ/C_{5870}					
	λ_{5300}	λ_{5313}	λ_{5546}	λ_{5800}	λ_{5822}	λ_{6630}
0	0.95 ± 0.03	1.02 ± 0.07	0.99 ± 0.02	1.02 ± 0.05	1.02 ± 0.05	0.98 ± 0.12
3.05S	0.99 ± 0.04	1.00 ± 0.01	0.96 ± 0.05	1.00 ± 0.01	1.00 ± 0.02	0.95 ± 0.05
6.10S	1.03 ± 0.05	1.03 ± 0.02	0.98 ± 0.05	1.01 ± 0.02	1.02 ± 0.04	0.95 ± 0.06
9.15S	1.01 ± 0.05	1.02 ± 0.01	0.96 ± 0.06	0.99 ± 0.02	1.00 ± 0.02	0.93 ± 0.05
12.20S	1.01 ± 0.05	1.01 ± 0.01	0.97 ± 0.05	0.99 ± 0.02	0.99 ± 0.01	0.94 ± 0.06
15.25S	1.04 ± 0.05	1.04 ± 0.01	0.98 ± 0.05	1.00 ± 0.01	1.00 ± 0.02	0.92 ± 0.06
18.30S	1.01 ± 0.04	1.02 ± 0.02	0.98 ± 0.04	1.02 ± 0.03	1.01 ± 0.03	0.96 ± 0.07
24.40S	1.02 ± 0.05	1.03 ± 0.02	1.00 ± 0.02	1.01 ± 0.02	1.01 ± 0.02	0.94 ± 0.07
3.05N	0.99 ± 0.06	0.99 ± 0.01	0.95 ± 0.05	0.99 ± 0.01	1.01 ± 0.03	0.95 ± 0.05
6.10N	0.99 ± 0.04	1.00 ± 0.02	0.95 ± 0.06	1.00 ± 0.01	1.01 ± 0.03	0.94 ± 0.05
9.15N	1.00 ± 0.05	1.00 ± 0.02	0.97 ± 0.04	1.00 ± 0.01	0.99 ± 0.02	0.94 ± 0.05
12.20N	1.00 ± 0.04	1.00 ± 0.03	0.97 ± 0.01	0.99 ± 0.03	1.01 ± 0.02	0.95 ± 0.06
15.25N	1.02 ± 0.05	1.02 ± 0.01	0.98 ± 0.05	1.01 ± 0.01	1.01 ± 0.01	0.95 ± 0.06
18.30N	1.00 ± 0.06	1.00 ± 0.02	0.97 ± 0.02	1.00 ± 0.01	1.00 ± 0.02	0.94 ± 0.05
24.40N	1.01 ± 0.05	1.01 ± 0.01	1.01 ± 0.04	1.00 ± 0.01	0.99 ± 0.01	0.93 ± 0.04

Table Notes. N and S correspond to north and south respectively.

increases from 2.30 Å in the center to ∼3.57 Å in the external regions. This result is in reasonable agreement with Carollo et al. (1993) who found no correlation of the Mg 2 index with either Fe I$_{5270}$ and Fe I$_{5335}$. In Fig. 4 we plot the velocity dispersion corrected values of the Mg 2 index *vs.* the EWs of Fe I$_{5270}$ and Fe I$_{5335}$, in which we see no correlation between these features. The different slope of the Mg 2 gradient relative to those of Fe I$_{5270}$ and Fe I$_{5335}$ can be accounted for by an enhancement of α-elements in general, Mg in particular (Faber et al. 1992 and Worthey et al. 1994). In NGC 5044 this effect is more intense in the center than in the outer regions.

The dependence of metallicity gradients on fundamental parameters was investigated by Carollo et al. (1993) who found that the Mg 2 gradient shows a bimodal trend. For objects with masses lower than $10^{11}\,M_\odot$, the Mg 2 gradient slope correlates with galaxy mass, whereas for objects more massive than $10^{11}\,M_\odot$, no such correlation appears.

In order to compare our results with the data of Carollo et al. (1993), first we estimate the mass of NGC 5044 us-

ing Poveda's approximation, $M_{tot} = 0.9\frac{\sigma^2 R_e}{G} = 3.34 \times 10^8\,M_\odot$, where G is the gravitational constant, $R_e = 28.53''$ is the effective radius and $\sigma = 256\,km\,s^{-1}$ is the central stellar velocity dispersion. According to Fig. 11 of Carollo et al. (1993), the calculated mass value of NGC 5044 together with the slope of the Mg 2 gradient, suggest that this elliptical galaxy was formed by a monolitic collapse.

On the other hand, Kobayashi et al. (1999) have examined line-strength gradients in 80 elliptical galaxies. They found typical gradients $\delta[Fe/H]/\delta log(r) \sim -0.3$, which are flatter than the ones predicted by monolithic collapse simulations. In this paper we found, using the same method, $\delta[Fe/H]/\delta log(r) = -0.31$ which is very close to the value obtained by Kobayashi et al. (1999).

3.2. [Fe/H] abundance

In order to estimate the [Fe/H] abundance in NGC 5044, we use the calibrations Mg 2 *vs.* [Fe/H], Fe I$_{5270}$ *vs.* [Fe/H] and Fe I$_{5335}$ *vs.* [Fe/H] presented by Worthey et al. (1992)
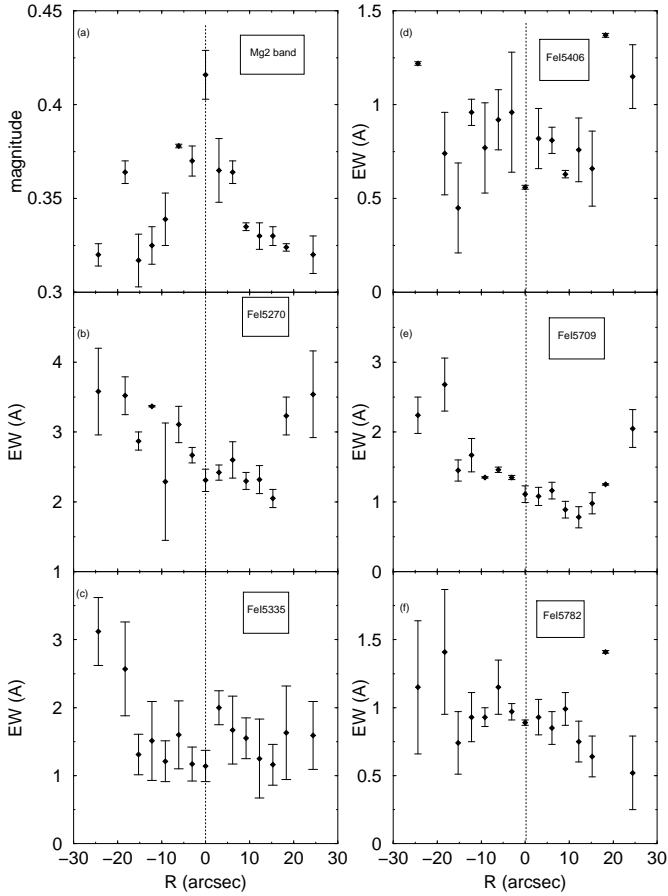
Fig. 3. Spatial variation of absorption features in NGC 5044.

Fig. 4. Mg 2 index vs. Fe I$_{5270}$ and Fe I$_{5335}$ line strength.

which are based on models of galactic globular clusters with 18 Gyrs of age. From Figure 1 of Worthey et al. (1992) we found that for our corrected Mg 2 index, [Fe/H]= 0.5 and 0.17 in the central and external regions, respectively. In the same way, using Fe I$_{5270}$ we found [Fe/H] = -0.5, 0.2; and for Fe I$_{5335}$, we found [Fe/H] = -1.0, -0.5 in the central and external regions, respectively. Therefore, we found an [Fe/H] abundance above solar using as metallicity indicator the Mg 2 index, while [Fe/H] is lower than solar for Fe I$_{5270}$ and Fe I$_{5335}$ lines; in addition Mg is above solar in NGC 5044.

4. Stellar population synthesis

For a good understanding of some properties of NGC 5044, such as the presence of central gas emission, a precise determination of the star formation process is necessary. Therefore, the age of the constituent stars in NGC 5044 is an important parameter to be determined.

The integrated spectrum of a given galaxy contains significant information on its stellar content and chemical enrichment (Bica & Alloin, 1985). In principle, this information together with a stellar population synthesis method, can be used to determine the star formation history (Bica & Alloin, 1986). In this work we employ the stellar population synthesis method developed by Bica (1988) which
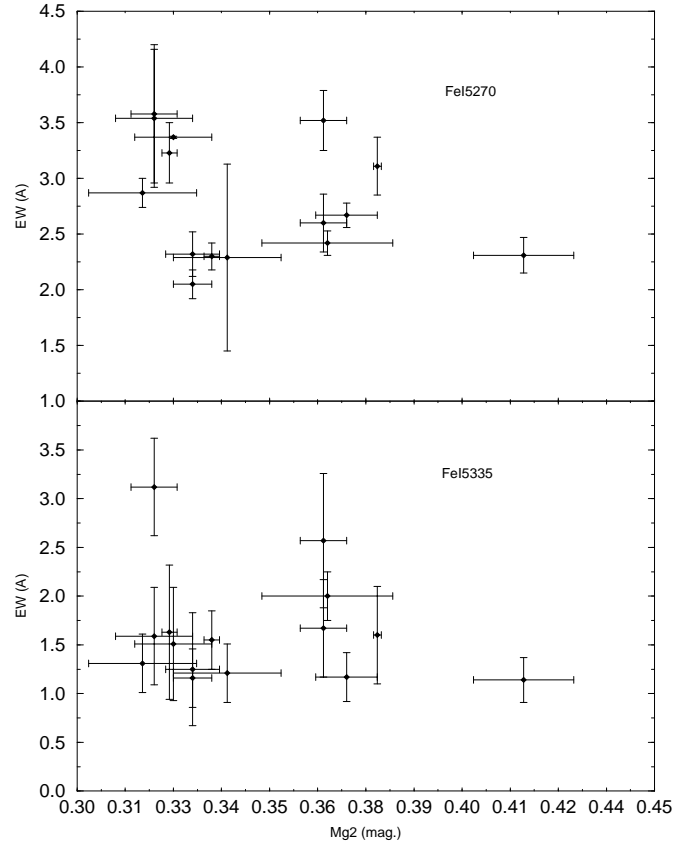
is based on integrated spectra of star clusters and H II regions, characterized by different ages and metallicities. In the present case, due to the small number of observational constraints (EWs and continuum points), we use three old components with different metallicities in order to minimize the degeneracy between age and metallicity of the different population components. These metallicities components (templates) are: $G1 \rightarrow [Z/Z_\odot] \sim 0.0$, $G2 \rightarrow [Z/Z_\odot] \sim -0.4$ and $G3 \rightarrow [Z/Z_\odot] \sim -1.1$, the three with age 10^{10} years.

Alternatively, we have also performed a stellar population synthesis with a set of three components with similar (solar) metallicities and different ages: G1 (10^{10} yr), Y3 (10^8 yr) and RHII (10^6 yr). We found that the spectra presented in Fig. 2 are better fitted by a range in metallicities than a range in ages. The base elements that we use are taken from the star cluster population templates described in Bica & Alloin (1986), and are presented in Fig. 5. The corresponding EWs and continuum points for the base elements have been measured similarly as those for NGC 5044 and are given in Tables 6 and 7, respectively. We remind that, for the stellar population analysis we use the EW of Mg 2, which is given in column (3) of Table 4.

Basically the algorithm uses the selected EWs and pivot points for the continuum measured in a given spectrum and compares them to those of a model computed from a base of simple stellar population elements. The
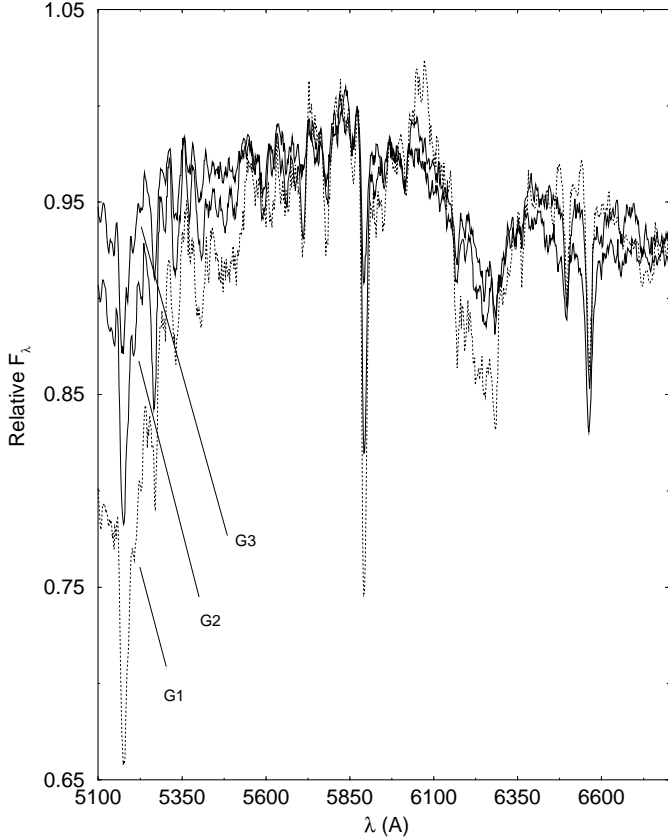
Fig. 5. Population templates (age components) used in the synthesis, normalized at $\lambda 5870\,\text{Å}$.

Table 6. Equivalent widths for the base

	Metallicity $[Z/Z_\odot]$	Mg 2_{band}	Fe I$_{5270}$	Fe I$_{5335}$	Fe I$_{5406}$	Fe I$_{5709}$	Fe I$_{5782}$
		EW (Å)					
$G1$	~ 0.0	5.82	2.77	1.65	1.50	1.36	1.14
$Y3$	~ -0.4	4.29	2.99	1.70	1.46	1.30	0.80
$Y3$	~ -1.1	2.75	1.59	0.95	0.77	0.57	0.52

Table 7. Continuum points for the base

	$\lambda 5300$	$\lambda 5313$	$\lambda 5546$	$\lambda 5800$	$\lambda 5822$	$\lambda 6630$
	C_λ/C_{5870}					
$G1$	0.91	0.97	1.01	1.01	1.00	0.94
$G2$	0.97	0.98	0.99	1.01	1.00	0.94
$G3$	0.97	0.99	0.99	0.99	1.00	0.93

to the flux at $\lambda 5870\,\text{Å}$. The values of $E(B-V)_i$ are also given in the table.

The G1 component ($[Z/Z_\odot] \sim 0.0$) dominates the $\lambda 5870\,\text{Å}$ flux in the central extractions of NGC 5044. In the nucleus, the G1 component contributes with $\sim 42\%$ of the total flux, while in the external regions the contribution decreases to $\sim 8.0\%$.

The G2 component ($[Z/Z_\odot] \sim -0.4$) contributes with $\sim 32\%$ in the central region, and $\sim 55\%$ in the external regions (24.40″). The G3 component ($[Z/Z_\odot] \sim -1.1$) contributes with $\sim 26\%$ in the central region, and $\sim 37\%$ in the external regions, as can be seen in Table 8. Flux fractions and the internal reddening as a function of distance to the center are shown in Fig. 7. Notice that the spatial distribution of the internal reddening $E(B-V)_i$ along the north and south directions (Table 8 and panel (d) in Fig. 7) does not characterize a gradient.

The spectra representing the stellar population of NGC 5044 have been constructed using the star cluster templates (Sect. 4) combined according to the proportions given by the synthesis. We illustrate this procedure in Fig. 6 in which we show the synthesis for the central extraction (top panel). The resulting pure emission spectrum, which is obtained after the subtraction of the population template, is shown in the bottom panel.

The goodness of the above stellar population synthesis method can be assessed by the residuals both in the EWs and continuum points. As can be seen in Table 9, most of the absorption features are reasonably well reproduced by the synthesis method. The residuals are almost equally distributed between positive and negative ones, probably indicating that NGC 5044 has the same metallicity than that of the templates. The continuum fit is quite good as well, as can be seen by the residuals in Table 10.

5.1. Integrated Colour Index

In order to put NGC 5044 in the context of other elliptical galaxies rich in interestellar medium, we build the colour-colour diagram (J-K) vs. (V-K), using the J, K and V photometric data for a sample of elliptical galaxies from Rembold et al. (2002) and NED. The results are presented

algorithm is not a minimization procedure, instead it generates all combinations of the base elements according to a given flux contribution step. The code also successively dereddens galaxy input continuum points and compares them against a given base model. Every combination is subsequently tested against a set of windows of maximum allowed difference between the observed and the resulting features obtained. Finally, the solutions satisfying all feature windows are averaged out, and this average is adopted as the final synthesis solution.

Initially we used a 10% step for testing flux contribution at $\lambda 5870\,\text{Å}$ generating about $\sim 5\,200$ combinations for each assumed $E(B-V)_i$. Reddenings were tested in the range $0.00 \le E(B\text{-}V)_i \le 0.50$ with a step of 0.01. Thus, in total, $\sim 260\,000$ combinations are tested for each extraction, and the number of possible solutions amounts to less than 1%. After probing as above the space of combinations, we calculate the solution with finer steps of 5%, 2% and finally 1%. We tested the Galactic (Seaton 1979), LMC (Fitzpatrick 1986) and SMC (Prévot et al. 1984) reddening laws for the synthesis of each extraction, and concluded that the Galactic law applies in all cases.

5. Synthesis results

The results of our synthesis are given in Table 8, where we present the percentage contribution of each base element
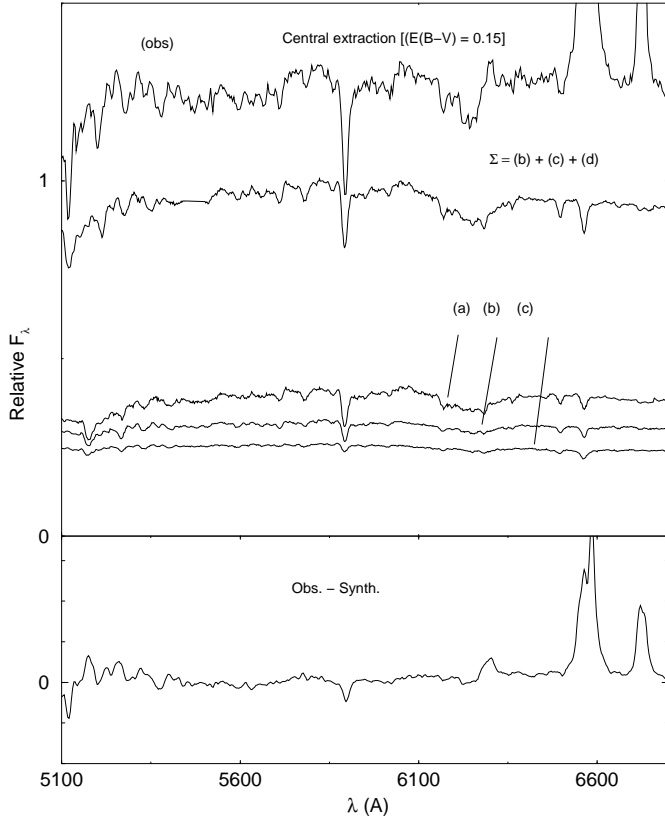
Fig. 6. Stellar population synthesis of the central extraction. Top panel: (obs) - observed spectrum corrected for reddening; (a) - G1 population template; (b) - G2 population template; (c) - G3 population template and ($\sum$) - synthesized spectrum. Bottom panel: pure emission spectrum. Spectrum (obs) has been shifted by a constant.

Fig. 7. Synthesis results in flux fractions as a function of distance to the center - Panels (a), (b) and (c); panel (d) - spatial distribution of the internal reddening.

Table 8. Synthesis results in terms of flux fractions

R ($''$)	Flux fraction at $\lambda 5870$ Å			
	G1 (%)	G2 (%)	G3 (%)	$E(B-V)_i$
0.00	41.31 ± 1.56	32.53 ± 2.30	26.16 ± 1.27	0.01
3.05 S	23.43 ± 2.04	42.29 ± 2.40	34.29 ± 0.88	0.00
6.10 S	20.27 ± 2.85	43.09 ± 2.96	36.64 ± 0.73	0.01
9.15 S	23.79 ± 1.76	32.46 ± 2.27	43.75 ± 1.2	0.01
12.20 S	27.04 ± 3.09	70.48 ± 3.01	2.48 ± 0.98	0.00
15.25 S	11.13 ± 2.79	44.95 ± 3.40	43.92 ± 1.45	0.02
18.30 S	16.19 ± 2.42	42.53 ± 3.03	41.28 ± 1.10	0.01
24.40 S	9.57 ± 2.75	58.16 ± 3.14	32.27 ± 1.01	0.01
3.05 N	19.09 ± 3.17	45.17 ± 3.25	35.74 ± 0.74	0.01
6.10 N	24.92 ± 0.95	32.75 ± 1.53	42.33 ± 1.03	0.01
9.15 N	22.69 ± 2.53	37.93 ± 3.89	39.38 ± 2.13	0.01
12.20 N	22.43 ± 2.69	34.97 ± 4.29	42.60 ± 2.40	0.01
15.25 N	14.33 ± 1.49	84.00 ± 2.58	1.67 ± 1.49	0.00
18.30 N	11.52 ± 2.72	70.10 ± 2.84	18.38 ± 1.15	0.00
24.40 N	7.83 ± 1.88	49.64 ± 2.69	42.53 ± 1.20	0.00

Table Notes. Column 1: S and N indicate south and north directions, respectively; Column 5: internal reddening, corresponding to the Galactic law.

Table 9. Equivalent width residuals (Å)

R ($''$)	Mg 2_{band}	Fe I$_{5270}$	Fe I$_{5335}$	Fe I$_{5406}$	Fe I$_{5709}$	Fe I$_{5782}$
0.00	0.48	-0.21	-0.34	-0.73	-0.02	0.02
3.05 S	0.24	0.22	-0.26	-0.27	0.29	0.19
6.10 S	0.85	0.69	0.19	-0.29	0.41	0.38
9.15 S	0.80	-0.02	-0.15	-0.40	0.35	0.17
12.20 S	0.57	0.47	-0.16	-0.49	0.37	0.04
15.25 S	0.94	0.53	-0.05	-0.71	0.46	0.02
18.30 S	0.80	1.16	1.19	-0.44	1.67	0.66
24.40 S	0.32	1.07	1.67	-0.02	1.17	0.41
3.05 N	0.30	-0.45	0.58	-0.40	0.03	0.16
6.10 N	0.67	-0.20	0.30	-0.37	0.15	0.08
9.15 N	0.50	-0.46	0.16	-0.57	-0.14	0.22
12.20 N	0.79	-0.40	-0.12	-0.41	-0.22	0.01
15.25 N	0.08	-0.73	-0.52	-0.79	-0.32	0.20
18.30 N	0.18	-0.01	0.07	0.03	0.08	0.62
24.40 N	0.57	0.55	0.21	-0.02	1.05	0.19

Table Notes. Residuals correspond to the observed − synthesized values.

index, NGC 5044 also presents mid-IR (6.7 to $15\mu m$) dust emission (Ferrari et al. 2002).

6. Ionized gas

Emission gas has been detected in a large number of elliptical galaxies. However, the origin of this gas and the ionization source are not yet conclusively established. NGC 5044 presents conspicuous emission lines throughout

in Fig. 8, showing that NGC 5044 has the reddest (V-K) colour. This result is probably due to the fact that besides the old stellar population contribution to the (V-K) colour
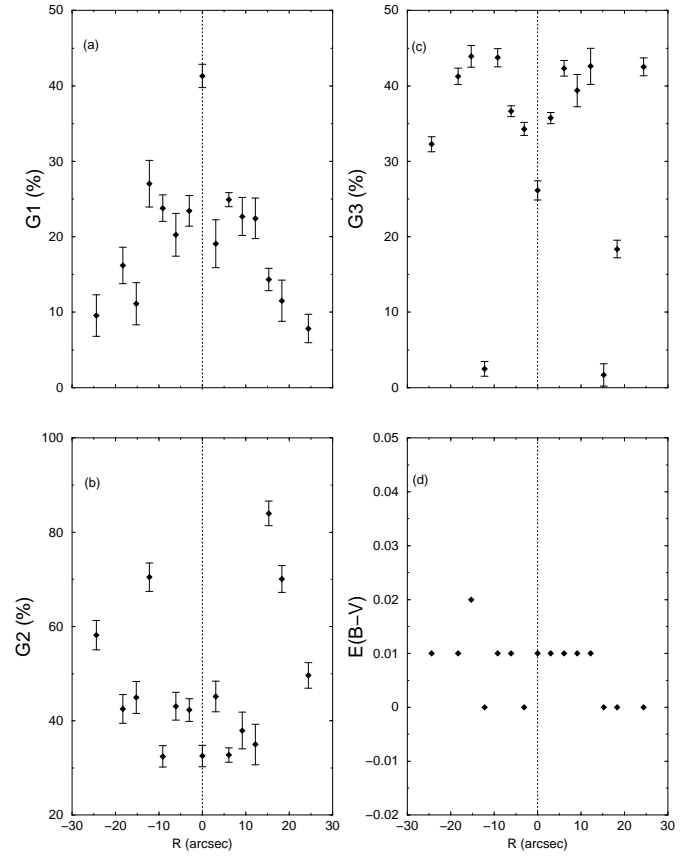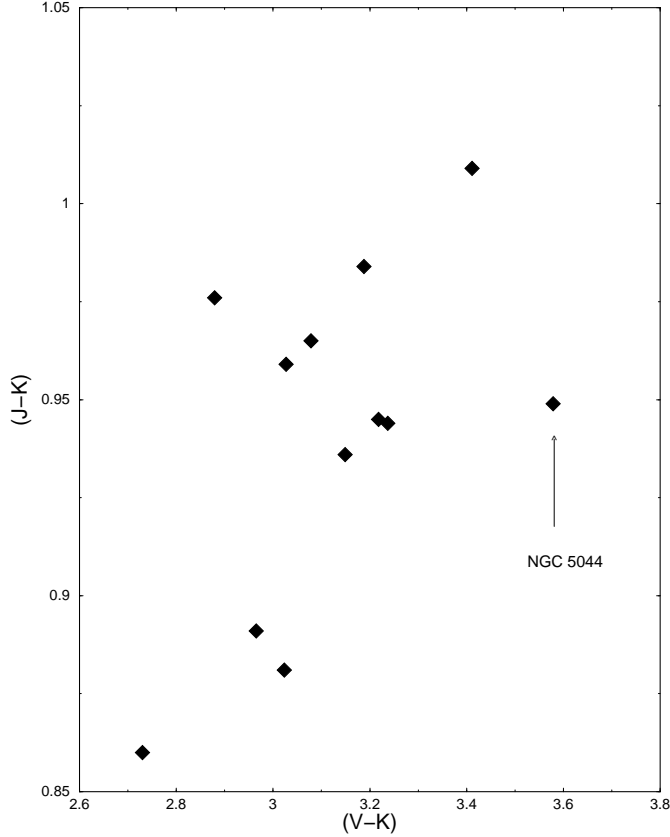
Table 10. Continuum residuals

R (″)	λ5300	λ5313	λ5546	λ5800	λ5822	λ6630
0.00	0.01	0.08	0.01	0.02	0.02	0.04
3.05 S	0.04	0.05	−0.02	0.01	0.00	0.01
6.10 S	0.08	0.08	0.00	0.02	0.02	0.01
9.15 S	0.06	0.07	−0.02	0.00	0.00	−0.01
12.20 S	0.06	0.06	−0.01	−0.01	−0.02	0.00
15.25 S	0.08	0.08	0.02	−0.01	0.00	−0.02
18.30 S	0.06	0.07	0.00	0.03	0.01	0.02
24.40 S	0.06	0.07	0.02	0.02	0.01	0.00
3.05 N	0.04	0.04	−0.03	0.00	0.01	0.01
6.10 N	0.04	0.05	−0.03	0.01	0.01	0.00
9.15 N	0.05	0.05	−0.01	0.01	−0.01	0.00
12.20 N	0.05	0.05	−0.01	0.00	0.01	0.01
15.25 N	0.06	0.06	0.00	0.02	0.00	0.01
18.30 N	0.04	0.04	−0.01	0.01	−0.01	0.00
24.40 N	0.04	0.04	−0.01	0.01	0.00	0.00

Table Notes. Residuals correspond to the observed − synthesized values.

Fig. 8. Colour-colour diagram (J-K) vs. (V-K)

Table 11. Emission line parameters.

$R('')$	lines	F_λ $(10^{-16}\,erg\,s^{-1}\,cm^{-2})$	$\frac{F_\lambda}{F_{H\alpha\,(R=0)}}$	$FWHM$ (Å)
0.00	$H\alpha$	6.80 ± 0.23	1.00	13.62
	$[NII]_{\lambda6548}$	22.0 ± 0.75	3.23 ± 0.15	21.27
	$[NII]_{\lambda6584}$	7.33 ± 0.25	1.07 ± 0.05	21.27
	$[SII]_{\lambda6717}$	8.73 ± 0.16	1.28 ± 0.04	23.64
	$[SII]_{\lambda6731}$	5.83 ± 0.11	0.85 ± 0.03	23.64
3.05S	$H\alpha$	4.29 ± 0.11	0.63 ± 0.03	11.82
	$[NII]_{\lambda6548}$	7.34 ± 0.19	1.08 ± 0.04	11.21
	$[NII]_{\lambda6584}$	2.44 ± 0.06	0.35 ± 0.01	11.21
	$[SII]_{\lambda6717}$	2.58 ± 0.08	0.37 ± 0.02	11.10
	$[SII]_{\lambda6731}$	1.96 ± 0.06	0.28 ± 0.01	11.10
6.10S	$H\alpha$	3.27 ± 0.14	0.48 ± 0.03	11.78
	$[NII]_{\lambda6548}$	5.91 ± 0.25	0.86 ± 0.04	12.24
	$[NII]_{\lambda6584}$	1.97 ± 0.08	0.28 ± 0.01	12.24
	$[SII]_{\lambda6717}$	2.04 ± 0.10	0.30 ± 0.02	10.73
	$[SII]_{\lambda6731}$	1.42 ± 0.07	0.21 ± 0.01	10.73
9.15S	$H\alpha$	2.91 ± 0.11	0.43 ± 0.02	15.08
	$[NII]_{\lambda6548}$	4.36 ± 0.17	0.64 ± 0.03	12.19
	$[NII]_{\lambda6584}$	1.45 ± 0.05	0.21 ± 0.01	12.19
	$[SII]_{\lambda6717}$	1.50 ± 0.08	0.22 ± 0.01	12.12
	$[SII]_{\lambda6731}$	1.24 ± 0.07	0.18 ± 0.01	12.12
12.20S	$H\alpha$	2.49 ± 0.09	0.37 ± 0.02	18.32
	$[NII]_{\lambda6548}$	2.36 ± 0.08	0.34 ± 0.01	12.59
	$[NII]_{\lambda6584}$	0.78 ± 0.03	0.11 ± 0.00	12.59
	$[SII]_{\lambda6717}$	0.60 ± 0.05	0.08 ± 0.01	11.12
	$[SII]_{\lambda6731}$	0.57 ± 0.04	0.08 ± 0.00	11.12
15.25S	$H\alpha$	3.39 ± 0.20	0.49 ± 0.03	32.46
	$[NII]_{\lambda6548}$	2.41 ± 0.14	0.35 ± 0.02	10.30
	$[NII]_{\lambda6584}$	0.80 ± 0.05	0.11 ± 0.01	10.30
	$[SII]_{\lambda6717}$	0.63 ± 0.03	0.09 ± 0.00	12.84
	$[SII]_{\lambda6731}$	1.15 ± 0.05	0.17 ± 0.01	12.84
18.30S	$H\alpha$	3.43 ± 0.13	0.50 ± 0.02	12.55
	$[NII]_{\lambda6548}$	5.47 ± 0.21	0.80 ± 0.04	11.88
	$[NII]_{\lambda6584}$	1.82 ± 0.07	0.26 ± 0.01	11.88
	$[SII]_{\lambda6717}$	1.00 ± 0.15	0.14 ± 0.02	10.26
	$[SII]_{\lambda6731}$	1.15 ± 0.17	0.17 ± 0.02	10.26
24.40S	$H\alpha$	4.06 ± 0.23	0.60 ± 0.04	17.73
	$[NII]_{\lambda6548}$	4.88 ± 0.27	0.71 ± 0.05	13.16
	$[NII]_{\lambda6584}$	1.62 ± 0.09	0.24 ± 0.01	13.16
	$[SII]_{\lambda6717}$	1.58 ± 0.21	0.23 ± 0.03	12.98
	$[SII]_{\lambda6731}$	1.09 ± 0.14	0.16 ± 0.02	12.98
3.05N	$H\alpha$	4.73 ± 0.38	1.13 ± 0.06	11.08
	$[NII]_{\lambda6548}$	7.84 ± 0.62	1.15 ± 0.10	11.85
	$[NII]_{\lambda6584}$	2.61 ± 0.21	0.38 ± 0.03	11.85
	$[SII]_{\lambda6717}$	2.32 ± 0.45	0.34 ± 0.06	10.73
	$[SII]_{\lambda6731}$	1.63 ± 0.32	0.24 ± 0.05	10.73
6.10N	$H\alpha$	3.74 ± 0.14	0.55 ± 0.02	11.08
	$[NII]_{\lambda6548}$	4.56 ± 0.23	0.67 ± 0.04	12.11
	$[NII]_{\lambda6584}$	1.52 ± 0.08	0.22 ± 0.03	12.11
	$[SII]_{\lambda6717}$	0.96 ± 0.07	0.14 ± 0.01	10.61
	$[SII]_{\lambda6731}$	0.70 ± 0.05	0.10 ± 0.01	10.61
9.15N	$H\alpha$	2.08 ± 0.11	0.30 ± 0.02	11.32
	$[NII]_{\lambda6548}$	3.51 ± 0.19	0.51 ± 0.03	12.80
	$[NII]_{\lambda6584}$	1.17 ± 0.06	0.17 ± 0.01	12.80
	$[SII]_{\lambda6717}$	0.72 ± 0.06	0.10 ± 0.01	11.35
	$[SII]_{\lambda6731}$	0.63 ± 0.05	0.09 ± 0.00	11.35
12.20N	$H\alpha$	1.25 ± 0.10	0.18 ± 0.01	11.74
	$[NII]_{\lambda6548}$	2.65 ± 0.21	0.39 ± 0.03	15.85
	$[NII]_{\lambda6584}$	0.88 ± 0.77	0.13 ± 0.01	15.85
	$[SII]_{\lambda6717}$	0.50 ± 0.02	0.07 ± 0.00	11.00
	$[SII]_{\lambda6731}$	0.40 ± 0.01	0.06 ± 0.00	11.00
15.25N	$H\alpha$	3.51 ± 0.17	0.51 ± 0.03	33.26
	$[NII]_{\lambda6548}$	2.41 ± 0.12	0.35 ± 0.02	10.31
	$[NII]_{\lambda6584}$	0.80 ± 0.04	0.12 ± 0.00	10.31
	$[SII]_{\lambda6717}$	0.40 ± 0.09	0.06 ± 0.01	10.89
	$[SII]_{\lambda6731}$	0.37 ± 0.08	0.05 ± 0.01	10.89
18.30N	$H\alpha$	1.32 ± 0.09	0.19 ± 0.01	11.45
	$[NII]_{\lambda6548}$	1.93 ± 0.13	0.28 ± 0.02	11.88
	$[NII]_{\lambda6584}$	0.64 ± 9.22	0.09 ± 1.35	11.88
	$[SII]_{\lambda6717}$	0.54 ± 0.14	0.08 ± 0.02	8.76
	$[SII]_{\lambda6731}$	0.48 ± 0.13	0.07 ± 0.02	8.76
24.40N	$H\alpha$	3.98 ± 0.22	0.58 ± 0.03	11.66
	$[NII]_{\lambda6548}$	4.82 ± 0.27	0.71 ± 0.05	10.71
	$[NII]_{\lambda6584}$	1.60 ± 0.90	0.23 ± 0.13	10.71
	$[SII]_{\lambda6717}$	1.60 ± 0.13	0.23 ± 0.02	11.87
	$[SII]_{\lambda6731}$	1.95 ± 0.15	0.28 ± 0.02	11.87

Table Notes. Column 4: Flux normalized to the central region $F_{H\alpha}$; Column 5: FWHM according to a gaussian fit.

the its body. The mass of ionized gas in NGC 5044 is estimated between 10^3 and $10^5\,M_\odot$ (Macchetto et al. 1996). In this section we investigate the physical conditions and ionization source of the gas in NGC 5044 using the results of the stellar population synthesis.

The properties of the emission gas are derived from line fluxes, measured in the stellar population subtracted spectra (Section 5). The emission lines used in the analysis are: $H\alpha$, $[N\,II]_{\lambda6548}$, $[N\,II]_{\lambda6584}$, $[S\,II]_{\lambda6717}$ and $[S\,II]_{\lambda6731}$. In Tab. 11 we list, for each extraction region, the absolute flux, the flux relative to that of $H\alpha$ in the central region, and the FWHM for the above emission lines. The uncertainty attributed to each measured flux is based on a gaussian least-squares fit.

Assuming that the emission lines are formed only by recombination, the number of ionizing photons (Q(H)) can be calculated as

$$Q(H) = \frac{L_{H\alpha}}{h\nu_\alpha}\frac{\alpha_B(H^0,T)}{\alpha_{H\alpha}(H^0,T)}, \tag{1}$$

where the $H\alpha$ luminosity is $L_{H\alpha} = 4\pi D^2 F_{H\alpha}$, $\alpha_B(H^0,T)$ is the recombination coefficient summed over all energy levels, and $\alpha_{H\alpha}(H^0,T)$ is the recombination coefficient at $H\alpha$. With a Hubble constant of $H_0 = 75\,\mathrm{km\,s^{-1}\,Mpc^{-1}}$,

Table 12. Luminosity and ionizing photons

R($''$)	$L_{H\alpha}$ ($\times 10^{37}\,erg\,s^{-1}$)	$Q(H)$ ($\times 10^{50}\,photons\,s^{-1}$)
0.00	10.5 ± 0.07	2.62 ± 0.02
3.05S	6.65 ± 0.04	1.66 ± 0.01
6.10S	5.06 ± 0.04	1.20 ± 0.01
9.15S	4.51 ± 0.03	1.08 ± 0.01
12.20S	3.85 ± 0.03	0.93 ± 0.01
15.25S	5.25 ± 0.04	1.29 ± 0.01
18.30S	5.31 ± 0.03	1.32 ± 0.01
24.40S	6.29 ± 0.06	1.55 ± 0.02
3.05N	7.33 ± 0.09	1.81 ± 0.03
6.10N	5.79 ± 0.04	1.42 ± 0.01
9.15N	3.22 ± 0.03	0.78 ± 0.01
12.20N	1.93 ± 0.01	0.46 ± 0.00
15.25N	5.54 ± 0.04	1.33 ± 0.01
18.30N	2.04 ± 0.01	0.51 ± 0.00
24.40N	6.16 ± 0.04	1.52 ± 0.01

Fig. 9. Spatial distribution of line-ratios and Q(H).

the distance to NGC 5044 is $D = 36$ Mpc. $L_{H\alpha}$ and Q(H) values are given in Tab 12.

In order to infer on the spatial properties of the emission gas, we plot in Fig. 9 the line ratios $\frac{[\text{N\,II}]_{\lambda\lambda 6548,84}}{H\alpha}$ (panel (a)), $\frac{[\text{S\,II}]_{\lambda\lambda 6717,31}}{H\alpha}$ (panel (b)), $L_{H\alpha}$ (panel (c)), and Q(H) (panel (d)).

Table 13. H II region model

Spectral type	$\frac{M}{M_\odot}$	Number	$N_{\text{Ly}\,\alpha}$ ($\times 10^{48}\,photons\,s^{-1}$)
O5	30	20	2.00
	22	41	0.25
B0	17	75	0.082
	15	101	0.043
	13	142	0.015
	10	264	0.0021

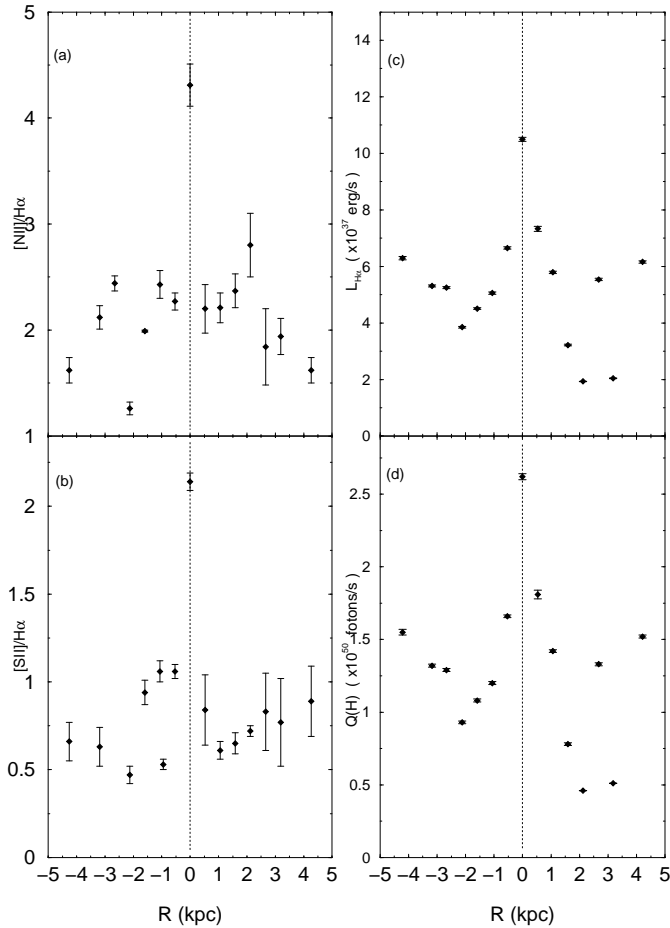Table Notes. Column 3: Number of stars of each spectral type.

In the central region, NGC 5044 presents $\frac{[\text{N\,II}]}{H\alpha} = 4.2$ and $\frac{[\text{S\,II}]}{H\alpha} > 1$. Notice that the ratio $\frac{[\text{N\,II}]}{H\alpha}$ is larger than 1.0 for all sampled regions (panel (a)).

In order to investigate the nature of the ionized source in the external regions of NGC 5044, we test two scenarios:

(i) the gas is ionized by an H II region. In order to reproduce the number of ionizing photons observed in the region at 3.05$''$, we have built an H II region according to a Salpeter initial mass function. The H II region model which best reproduces the observed number of ionizing photons is listed in Tab. 13, where we give the distribution of stars according to spectral type and mass; in the last column we give the number of Ly α photons produced by each star (Dottori 1991). This model H II region produces $\sim 2.59 \times 10^{50}$ photons s^{-1} which is comparable to the observed value. However, such an H II region in NGC 5044 would be bright enough to be photometrically detected in visible images obtained with the ESO 3.60302fig10.eps0302fig10.epsm telescope. The V-band image does not present any signature of such an H II region.

(ii) the gas is ionized by a hot, post-AGB star. The number of ionizing photons produced by one post-AGB star with effective temperature of $\sim 150\,000\,K$ corresponds to $\sim 6.11 \times 10^{50}$ photons s^{-1}, about 5 times the number of photons observed in the region at 3.05$''$. The spatial profiles of [N II] and H α extracted along the slit, shown in Fig. 10, reveal that $\frac{[NII]}{H\alpha} > 2$. However, according to the ionization models for old stars in elliptical galaxies (Binette et al. 1994) the ratio $\frac{N[\text{II}]}{H\alpha}$ measured in NGC 5044 could only be produced by a much larger Q(H) than the one we estimate, in particular the high value measured in the central region. Binette et al.'s (1994) models do not reproduce as well the observed ratio $\frac{[SII]_{6731}}{H\alpha}$. A high ratio $\frac{N[\text{II}]}{H\alpha}$ is characteristic of AGNs.

In conclusion we find that in the central region the ionization source must be a AGN, while in the external region the lower ratio $\frac{N[\text{II}]}{H\alpha} \sim 2$ can be accounted for by post-AGB stars.

7. Conclusions

The stellar population, metallicity distribution and ionized gas in NGC 5044 have been investigated in this paper by means of long-slit spectroscopy and stellar population synthesis. With respect to the spatial distribution of
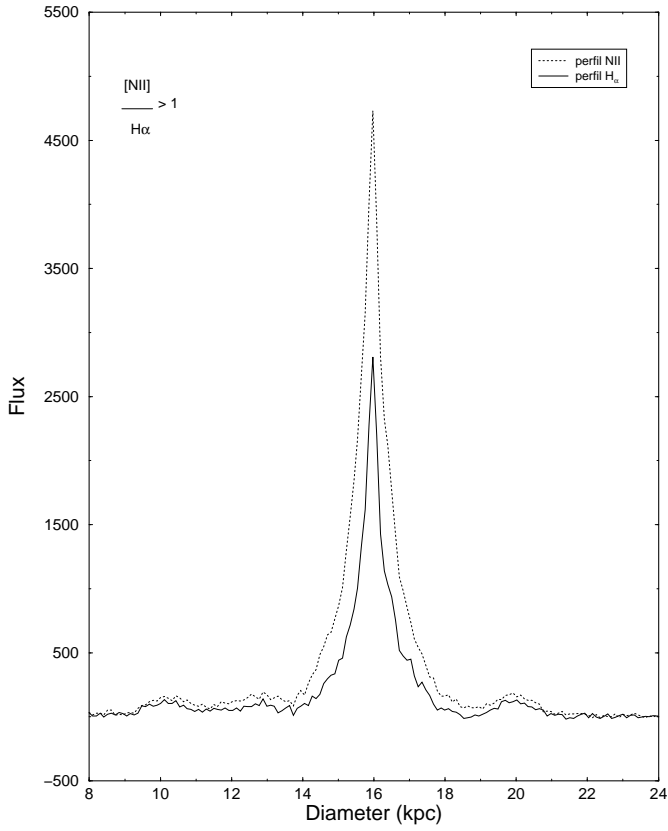
Fig. 10. Spatial profiles of H α and [NII]. Notice that [NII]/H$_\alpha$ > 1 along the galaxy.

metal-strength indices (corrected for velocity dispersion), the Mg 2 profile increases towards the central region, contrary to what is observed for the profile of Fe I$_{5270}$. This difference in slopes may be accounted for by an enhancement of α-elements in general, Mg in particular. The Mg 2 gradient slope compared with the mass of NGC 5044 indicates a monolitic collapse. However, the measure [Fe/H] gradient slope is not characteristic of one monolitic collapse.

The stellar population synthesis gives that most metallic component ($[Z/Z_\odot] \sim 0.0$) dominates the $\lambda 5870\,\text{Å}$ flux in the central region of NGC 5044. In the nucleus, this component contributes with $\sim 42\%$ of the total flux, while in the external regions the contribution decreases to $\sim 8.0\%$. The component with $[Z/Z_\odot] \sim -0.4$ contributes with $\sim 32\%$ in the central region, and $\sim 55\,\%$ in the external regions. The metal-poor component ($[Z/Z_\odot] \sim -1.1$) contributes with $\sim 26\,\%$ in the central region, and $\sim 37\,\%$ in the external regions. The spatial distribution of the internal reddening E(B−V)$_i$ along the north and south directions does not characterize a gradient.

The large values of the ratio $\frac{[\text{N\,II}]}{H\alpha}$ observed in all sampled regions characterizes the presence of a non-thermal ionization source, such as a low-luminosity AGN and/or shock ionization. However, in the external regions an additional ionization source is necessary to explain the emission lines, which might be hot, post-AGB stars.

References

Bica, E. 1988, A&A, 195, 79

Bica, E., Arimoto, N. & Alloin, D. 1988, A&A, 202, 8

Caon, N., Macchetto, D., Pastoriza, M. 2000, ApJS, 127, 39

Carollo, C. M., Danziger, I.J., Buson, L. 1993, MNRAS, 265, 553

Carollo, C. M., Danziger, I.J., Buson, L. 1993, MNRAS, 553, 580

Carollo, C. M., Danziger, I.J. 1994a, MNRAS, 270, 523

Carollo, C. M., Danziger, I.J. 1994b, MNRAS, 270, 743

Davies, R.L., Burstein, D., Dressler, A., Faber, S.M., Lynden-Bell, D., Terlevich, R., Wegner, G. 1987, ApJS, 64, 581

Davies, R.L., Sadler, E.M., Peletier, R.F. 1993, MNRAS, 262, 650

Davies, R.L., Sadler, E.M., Peletier, R.F. 1993, MNRAS, 650, 680

Dottori, H. A. 1981, Ap&SS, 80, 267

Fabbiano, G., Kim, D.-W., Trinchieri, G. 1992, ApJS, 80, 531

Faber, S. M., Friel, E. D., Burstein, D., Gaskell, C. M. 1985, ApJS, 57, 711

Faber, S.M., Worthey, G., Gonzáles, J.J. 1992, in IAU Symp. 149, B. Barbuy and A. Renzini (eds.), p.255

Ferguson, H.& Sandage, A. 1990, AJ, 100, 1

Ferrari, F., Pastoriza, M. G., Macchetto, F., Caon, N. 1999, A&A, 136, 269

Ferrari, F.; Pastoriza, M. G.; Macchetto, F. D.; Bonatto, C.; Panagia, N.; Sparks, W. B. 2002, A&A, 389, 355

Fitzpatrick, E.L. 1986, AJ, 92, 1068

Fisher, D., Franx, M., Illingworth, G. 1996, ApJ, 459, 110

Fisher, D., Franx, M., Illingworth, G. 1995, ApJ, 448, 119

Gonzáles J.J. 1993, Ph.D. thesis, Univ. California, Santa Cruz

Goudfrooij, P. 1991, ISSN, 63, 42

Kobayashi, C.,Arimoto, N. 1999, ApJS, 527, 599

Kurucz, R. L. 1979, ApJS, 40, 1

Macchetto, F., Pastoriza, M., Caon, N., Sparks, W.B., Giavalisco, M., Bender, R., Capaccioli, M. 1996, A&A, 120, 463

Matteucci, F. 1997, Fund. Cosmic Phys. 17, 283

Prévot, M.L., Lequeux, J., Maurice, E., Prévot, L. & Rocca-Volmerange, B. 1984, A&A, 132, 389

Rembold, S.B., Pastoriza, M. G., Ducati, J. R., Rubio, M., Roth, M. 2002, ApJ, 588, 344

Seaton, M.J. 1979, MNRAS, 187, 73p

Tantalo, R, Chiosi, C. Bressan, A., 1998, A&A, 333, 419

Worthey, G. 1994, ApJS, 95, 107

Worthey, G., Faber S.M., Gonzáles, J.J., Burstein, D. 1994, ApJS, 94, 687

Worthey, G.; Faber, S. M.; Gonzáles, J. J . 1992, ApJS, 398, 69